京都大学学術情報リポジトリ
KURENAI 紅
Kyoto University Research Information Repository

京都大学
KYOTO UNIVERSITY

Title	Encephalomyocarditis virus disrupts stress granules, the critical platform for triggering antiviral innate immune responses.
Author(s)	Ng, Chen Seng; Jogi, Michihiko; Yoo, Ji-Seung; Onomoto, Koji; Koike, Satoshi; Iwasaki, Takuya; Yoneyama, Mitsutoshi; Kato, Hiroki; Fujita, Takashi
Citation	Journal of virology (2013), 87(17): 9511-9522
Issue Date	2013-09
URL	http://hdl.handle.net/2433/178797
Right	© 2013, American Society for Microbiology.
Type	Journal Article
Textversion	author

Kyoto University

EMCV Disrupts Stress Granules, the Critical Platform for Triggering Antiviral Innate Immune Responses

Chen Seng Ng[1,2], Michihiko Jogi[1,2,3], Ji-Seung Yoo[1,2], Koji Onomoto[1,2,3], Satoshi Koike[4], Takuya Iwasaki[4], Mitsutoshi Yoneyama[1,2,3], Hiroki Kato[1,2], Takashi Fujita[1,2*]

[1]Laboratory of Molecular Genetics, Institute for Virus Research, Kyoto University, Kyoto 606-8507, Japan.

[2]Laboratory of Molecular Cell Biology, Graduate School of Biostudies, Kyoto University, Kyoto 606-8507, Japan.

[3]Division of Molecular Immunology, Medical Mycology Research Center, Chiba University, Chiba 260-8673, Japan

[4]Neurovirology Project, Tokyo Metropolitan Institute of Medical Science, Tokyo 156-8506, Japan

***Corresponding author. Mailing address:**

Takashi Fujita
Laboratory of Molecular Genetics,
Institute for Virus Research,
Kyoto University,
Kyoto 606-8507,
JAPAN.

Phone and Fax: (+81)-75-751-4031
E-mail: tfujita@virus.kyoto-u.ac.jp

Running title: Loss of stress granule impaired interferon signals.

Abstract word count: 244 words

Text word count: 4,198 words

38 **ABSTRACT**
39
40 In response to stress, cells induce ribonucleoprotein aggregates, termed stress granules (SGs).
41 SGs are transient loci containing translation-stalled mRNA, which is eventually degraded or
42 recycled for translation. Infection of some viruses including influenza A virus with a
43 deletion of non-structural protein 1 (IAVΔNS1) induces SG-like protein aggregates.
44 Previously, we showed that IAVΔNS1-induced SGs are required for efficient induction of
45 type I interferon (IFN). Here, we investigated SG formation by different viruses using
46 GFP-tagged Ras-GAP SH3 domain binding protein-1 (GFP-G3BP1) as an SG probe. HeLa
47 cells stably expressing GFP-G3BP1 were infected with different viruses and GFP
48 fluorescence was monitored live with time-lapse microscopy. SG formation by different
49 viruses was classified into 4 different patterns: no SG formation, stable SG formation,
50 transient SG formation and alternate SG formation. We focused on EMCV infection, which
51 exhibited transient SG formation. We found that EMCV disrupts SGs by cleavage of G3BP1
52 at late stages of infection (>8 h) through a similar mechanism to that by poliovirus.
53 Expression of a G3BP1 mutant, which is resistant to the cleavage, conferred persistent
54 formation of SG as well as an enhanced induction of IFN and other cytokines at late stages of
55 infection. Additionally, knockdown of endogenous G3BP1 blocked SG formation with
56 attenuated induction of IFN and potentiated viral replication. Taken together, our findings
57 suggest a critical role of SG as an antiviral platform and shed light on one of the mechanisms
58 by which a virus interferes with host stress and subsequent antiviral responses.

59

60 **Keywords:** Encephalomyocarditis virus, melanoma differentiation-associated protein 5,
61 stress-granules, G3BP1**,** interferon

62 **INTRODUCTION**
63
64 In eukaryotic cells, viral infections induce several responses. Cellular pathogen recognition
65 receptors such as RIG-I-like receptors (RLRs), and Toll-like-receptors recognize specific
66 pathogen-associated molecular patterns and activate the transcription of hundreds of genes
67 including interferons (IFNs), inflammatory cytokines and antiviral proteins. Secreted IFNs, in
68 turn, activate a secondary JAK-STAT signaling cascade, which culminate in the activation of
69 various interferon stimulated genes (ISGs) (1,2). A representative ISG, protein kinase
70 RNA-activated (PKR), acts as an antiviral protein by inducing the blockade of viral
71 translation (3-5). PKR is also known to associate with cellular stress-responses. Virus
72 infection results in the accumulation of double-stranded RNA (dsRNA), thereby activating
73 PKR and phosphorylation of eukaryotic initiation factor 2α (eIF2α), leading to the formation
74 of stress granules (SGs) (6,7). Several studies have reported about the interaction between
75 viruses and SGs, especially the effects of specific type of viruses on the fate of SG formation
76 and how viruses modulate stress granule assembly (8-11). Recently, we reported that RLR
77 recruitment to SGs during SG formation is critical in RLR-mediated signaling and
78 non-structural protein 1 of influenza A virus blocks RLR signaling by inhibiting SG and
79 antiviral response (12). Accumulating evidence suggests that viruses have evolved strategies
80 to prevent SG formation. These results suggest that virus-induced SGs potentially serve as
81 platforms for antiviral activity, however, the underlying molecular mechanism still remains to
82 be elucidated.

83 In the present study, we aim to delineate the physiological impact of stress granule
84 formation and its viral modulation. We employed an EGFP-tagged stress granule marker,
85 Ras-Gap-SH3 domain binding protein (G3BP1) to probe the subcellular distribution of
86 virus-induced SGs (13,14). This system allows us to monitor SGs in an individual
87 virus-infected cell. Infection with RNA and DNA viruses displayed three distinct patterns:

88 stable, transient and alternate formation of SG. We focused on encephalomyocarditis virus
89 (EMCV), which exhibited transient formation of SGs. We show that EMCV disrupts SGs
90 through G3BP1 cleavage. Furthermore, we found that EMCV-induced SGs are required for
91 efficient activation of IFN and cytokine genes. We propose a new antiviral concept
92 highlighting the potential cross-talk of virus-induced stress responses and activation of the
93 IFN signaling cascade. This may provide a new insight in understanding the mechanism by
94 which antiviral genes are regulated.

95

96

97 **MATERIALS AND METHODS**
98
99
100 **Plasmid constructs.** The stress granule marker constructs pEGFP-C1-G3BP1 (NM_005754)
101 was a kind gift from Dr. Jamal Tazi (Institute de Génétique Moléculaire de Montpellier,
102 France). pEGFP-C1-G3BP1 Q325E mutant construct was generated by site-directed
103 mutagenesis through KOD-Plus-Mutagenesis kit (TOYOBO, Japan), using primers
104 containing the desired mutation according to manufacturer's instructions, and were
105 completely sequenced by using ABI Prism DNA sequencer to verify the presence of mutation.
106 This plasmid contained a single point amino acid substitution at position 325 (from glutamine
107 to glutamate), which is resistant to cleavage by $3C^{PRO}$ of Poliovirus (PolioV) (15).
108 Expression vectors for EMCV pF-leader and pF-3C protease were described previously (16).
109
110 **Viruses.** PolioV (Mahoney strain), vesicular stomatits virus (VSV, Indiana strain), EMCV,
111 adenoviruses (Type5), Sindbis virus (SINV) and Theiler's murine encephalomyelitis virus
112 (TMEV, GDVII strain) were prepared by infecting BHK cells at a multiplicity of infection
113 (MOI) of 1. Cell culture medium was collected after confirming cytopathic effects following
114 infection. Medium containing newly produced viruses was centrifuged at 1,500rpm for 5 min
115 to pellet down the cell debris, supernatant containing viruses were collected and stored at
116 -80°C. Viral titer was assessed by plaque assay on L929 cells as previously described (17).
117 NDV (Miyadera strain), Sendai virus (Cantell, SeV) and influenza A virus with a deletion of
118 the NS1 gene (IAVΔNS1, strain A/Puerto Rico 8/34) (18,19) were propagated in the allantoic
119 cavities of embryonated chicken eggs, then stocks were stored at -80°C.

120

121 **Generation of stable HeLa cells and general cell culture conditions.** Cell lines were
122 maintained in Dulbecco's Modified Eagle's medium (DMEM) supplemented with 10%

123 heat-inactivated fetal bovine serum (Nacalai Tesque, Japan) and Penicillin-Streptomycin
124 (100U/mL and 100μg/mL respectively, Nacalai Tesque, Japan). To generate HeLa cells
125 stably expressing EGFP-G3BP1 wild type and Q325E mutant, pEGFP-C1-G3BP1 and
126 pEGFP-C1-G3BP1 Q325E mutant expression constructs was linearized by restriction enzyme
127 ApaL1 (Takara, Japan). The linearized plasmids were then transfected into HeLa cells using
128 FuGENE6 (Promega, USA) according to manufacturer's recommendations. Transformants
129 were selected by including 1 mg/mL of G418 in the culture medium. Individual colonies
130 were isolated and characterized.
131
132 **Live-cell imaging and immunofluorescence microscopy.** For the live-cell imaging
133 analysis, HeLa cells stably expressing EGFP-G3BP1 (HeLa/G-G3BP) were seeded in 12-well
134 plate and incubated at 37°C. After 24 hours, cells were washed with DMEM medium (10%
135 fetal bovine serum and 1% Penicillin-Streptomycin) for several rounds. Cells were then
136 infected with various types of RNA and DNA viruses. After 1 hour infection, virus was
137 removed and replaced with 1.0 mL of DMEM imaging medium (4,500 mg/L D-glucose and
138 L-glutamine, 25mM HEPES buffer, no sodium pyruvate and phenol red, Invitrogen). Imaging
139 was immediately initiated every 10mins. Live cells were maintained on the microscope stage
140 at 37°C, with 5% carbon-dioxide in a humidity-controlled chamber. Images were mounted
141 using Biophotonics-ImageJ software. All imaging was performed by using a Leica CTR
142 6500.
143 For the immunofluorescence analysis, cells were seeded either in a 12-well plate or a
144 8-well chamber slide and incubated at 37°C. After 24 hours, cells were subjected to various
145 treatments such as plasmid transfection or virus infection. Cells were then rinsed in
146 phosphate-buffered saline (PBS) several times, fixed with 4% paraformaldehyde solution for
147 10 min at room temperature, washed with PBS for two additional rounds, permeabilized with

148 acetone:methanol (1:1) for one minute, and blocked with phosphate-buffered saline
149 containing 0.1 % Tween-20 (PBST) solution containing bovine serum albumin (BSA, 5.0
150 mg/mL) for 1 hour at 4°C. Cells were then incubated with primary antibody, followed by
151 fluorophores-conjugated secondary antibodies (Invitrogen) for one-hour at 4°C. Cells were
152 washed with PBST extensively and mounted. All images were obtained by a Leica CTR
153 6500.

154

155 **siRNA-directed gene silencing.** The siRNA universal negative control and siRNA targeting
156 stress granule marker-G3BP1 (50nM) and dsRNA protein kinase PKR were purchased from
157 Invitrogen, and transfected using either Lipofectamine2000 (Invitrogen) or RNAiMax
158 (Invitrogen) according to manufacturer's recommendation. The sequence of siRNA: RIG-I,
159 sense 5'-CGG AUU AGC GAC AAA UUU AUU-3', antisense 5'-UAA AUU UGU CGC
160 UAA UCC GUU-3'; PKR#1, sense 5'-UUU ACU UCA CGC UCC GCC UUC UCG U-3',
161 antisense 5'-ACG AGA AGG CGG AGCGUGAAGUAA A -3'; PKR#2, sense 5'- AUG UCA
162 GGA AGG UCA AAU CUG GGU G-3', antisense 5'-CAC CCA GAU UUG ACC UUC CUG
163 ACA U-3'; G3BP1, sense 5'-UAA UUU CCC ACC ACU GUU AAU GCG C-3', antisense
164 5'-GCGCAUUAACAGUGGUGGGAAAUUA-3'. After 48 hours post-transfection, cells
165 were subjected to viral infection or other treatments. A specific antibody for G3BP1 (Santa
166 Cruz) was used to monitor the knockdown efficiency.

167

168 **RNA analysis.** RNA was harvested from cells with TRIzol (Invitrogen) according to the
169 manufacturer's instructions. Contaminating DNA was then eliminated by using recombinant
170 DNase I (Roche, 10 units/μL) according to the manufacturer's protocol. Treated samples
171 were purified by phenol-chloroform extraction. 500 ng of purified RNA was used as a
172 template to synthesize cDNA using a High Capacity cDNA Reverse-Transcription kit

173 (Applied Biosystem) as specified by the manufacturer through the following cycles: 25°C for
174 10 seconds; 37°C for 2 hours; 85°C for 10 seconds. The concentration of cDNA was
175 quantified by a spectrophotometer and the final concentration was adjusted to 1 μg/μL.
176 cDNA samples were then either subjected to standard PCR or real-time quantitative-PCR
177 analysis with specific probes from Taqman Gene Expression Assay (Applied Biosystem).
178 Quantification of EMCV viral RNA was performed using SYBR master mix (Applied
179 Biosystem) with specific primers targeting EMCV capsid coding region. Standard PCR was
180 performed with cDNA samples together with a master mix containing 1X PCR buffer,
181 2.5mM of each dNTP's, 0.2 units of ExTaq Polymerase and 1.0μM of both forward and
182 reverse primers. PCR buffer, dNTPs and ExTaq Polymerases were purchased from Takara,
183 Japan. Primers were all customized and purchased from Invitrogen. PCR was performed in
184 50 μL reaction mixture with initial annealing temperature at 56°C-60°C. PCR products were
185 analyzed by agarose gel electrophoresis.
186
187 **Western blotting.** Cells were collected in ice-cold PBS by scrapper. Cells were collected
188 by centrifugation and lysed by NP-40 buffer (50mM Tris [pH8.0], 150mM NaCl, 1%
189 [vol/vol] NP-40, 1 nM of Vanadate, 1 mM of Leupeptin and phenylmethanesulfonylfluoride),
190 followed by centrifugation at 15,000rpm for 10 min and ultracentrifugation at 100,000rpm for
191 5min. The supernatant was mixed with an equal volume of 2X SDS buffer, boiled for 5 min,
192 separated by SDS-PAGE (30μg/lane), and transferred to nitrocellulose membrane. The
193 membranes were incubated in blocking buffer (PBS, 5% [wt/vol] dry milk powder) for 30min
194 at room temperature, followed by incubation with primary antibody diluted in blocking buffer
195 at 4°C overnight. Membranes were washed extensively with TBST (TBS, 0.1% Tween-20),
196 followed by incubation with a conjugated-secondary antibody for 1 hour at room temperature.
197 The proteins were visualized using alkaline-phosphatase buffer containing BCIP-NBT

198 (Promega) color development substrate (100 mM Tris-HCl [pH9.0], 150 mM NaCl, 1 mM
199 $MgCl_2$, 66 µL of NBT [50 mg/mL] and 33 µL of BCIP [50mg/mL]).
200
201 **Antibodies.** The antibodies used in this study include mouse monoclonal anti-GFP (1:1000,
202 MBL); goat polyclonal anti-G3BP1 (1:500, Santa Cruz sc-70283); mouse monoclonal
203 anti-G3BP1 (1:1000, Santa Cruz sc-365338); rabbit polyclonal anti-PKR (1:1000, Santa Cruz
204 sc-709); rabbit polyclonal anti-TIA1/R (1:1000, Santa Cruz sc-48371); goat polyclonal
205 anti-TIAR (1:1000, Santa Cruz sc-1749); rabbit polyclonal anti-HuR (1:1000, Santa Cruz
206 sc-365816); Propidium iodide [PI] (1:2000 in PBST, Miltenyi Biotec). The RIG-I antibody
207 were generated by immunizing a rabbit with a synthetic peptide corresponding to amino acid
208 793-807 of RIG-I and MDA5. Mouse monoclonal anti-PABP (1:1000, Abcam ab6125);
209 rabbit monoclonal anti-actin (1:5000; BioLegend Poly6221); mouse anti-FLAG (1:1000,
210 Sigma Aldrich) and rabbit monoclonal anti-phospho-PKR pT446 (1:1000, Epitomics Inc.).
211 Anti-EMCV polyclonal antibody was obtained by immunizing a rabbit with purified EMCV
212 virions. Anti-MDA5 polyclonal antibody was obtained by immunizing a rat with recombinant
213 MDA5 (produced in insect cells) which was pre-activated with RNA ligands.
214
215 **Quantification for the distribution pattern of virus-induced SG.** SG formation was
216 quantified visually by using eye-sight counting. The total number of cells displaying each
217 unique distribution pattern in each location was recorded and the percentage for each pattern
218 was calculated. As for the fixed cells, 10 pictures at different locations were taken randomly.
219 Cells displaying SG foci were quantified manually. Graphs display the average percentage of
220 replicates (at least 20 times).
221
222
223

224 **RESULTS**
225
226 **Characterization of HeLa cells stably expressing SG marker, G3BP1.** To monitor SGs in
227 living cells, we generated HeLa/G-G3BP (Fig. 1). Constitutive aggregation of intrinsic SG
228 components is reported to lead to a severe stall in protein synthesis and eventual apoptosis
229 (14,20). All the HeLa/G-G3BP clones displayed uniform and high GFP expression and their
230 growth rate was comparable to the parental cells (our unpublished observation). It has been
231 well documented that G3BP1 accumulates in SG foci in response to arsenite treatment
232 (oxidative stress) and virus infection (12,13). HeLa/G-G3BP clone 12 was treated with
233 arsenite or infected with Newcastle disease virus (NDV) or Influenza A virus (IAV) with an
234 NS1 deletion (IAVΔNS1), then the GFP localization was examined by confocal microscopy.
235 As shown in Fig. 1A, speckle-like localization of GFP was induced by these stimuli. Other
236 clones also exhibited similar speckle formation after arsenite treatment or NDV infection (Fig.
237 1B, C). We confirmed that other SG components, TIA-1, TIAR, HuR and eIF3 colocalized
238 with the GFP speckles (unpublished observation). These results indicate that EGFP-G3BP1
239 acts as a suitable probe for virus-induced SGs. However, since transient overexpression of
240 G3BP1 results in SG formation without external stress (13), we tested if the HeLa/G-G3BP
241 clones would exhibit normal antiviral response. As shown in Fig. 1D, all clones exhibited
242 comparable induction of IFN-β mRNA as parental cells. We chose clone 18 for further
243 analyses.
244
245 **G3BP1 exhibits three redistribution patterns after infection with both RNA and DNA**
246 **viruses.** To examine the dynamics of cytoplasmic SGs induced by viral infection, the cells
247 were infected with different viruses as shown in Fig. 2 and monitored live for distribution of
248 GFP fluorescence (representative results are shown in Movie S1-S9). Cells infected with SeV,
249 IAV, VSV and TMEV did not show SG formation (8). Other viruses induced SGs, typically

250 forming a large number of small granules around 5 h post infection and gradually fusing to
251 each other. SG formation was quantified (Fig. 2A-K) and classified into three predominant
252 patterns: stable formation (Fig. 2L), transient formation (Fig. 2M), and alternating formation
253 (Fig. 2N) within a single cell. NDV, IAVΔNS1 and Adenovirus 5 displayed a stable
254 formation of SGs (Movie S1-S3). Whereas SINV, EMCV and PolioV induced foci at around
255 5 to 6 h post infection, however, the foci disappeared thereafter (transient formation) (Fig.
256 2D-2F; Movie S4-S6). Interestingly, adenovirus 5 with E1A deletion, exhibited multiple
257 rounds of formation and disappearance of SGs (alternate formation) in the majority of cells
258 (Fig. 2I; Movie S7). Similar oscillation of SGs in cells infected with HCV and treated with
259 IFN was reported (21). Collectively, these live-cell imaging analyses demonstrated that viral
260 infections trigger host stress responses, however different viruses induce distinct response
261 patterns, presumably through specific underlying mechanisms. The observed SG formation
262 patterns are unlikely due to G3BP1 overexpression because wt HeLa cells exhibited transient
263 SG formation upon EMCV infection when endogenous G3BP1 was used as a marker (Fig.
264 2O).
265
266 **EMCV infection results in the cleavage of G3BP1.** We focused on the mechanism of
267 transient formation of SGs by EMCV because PolioV has been reported to inhibit SG
268 formation by cleavage of G3BP1 (15). We examined if EGFP-G3BP1 is cleaved by EMCV
269 by Western blotting. EGFP-G3BP1 fusion protein is detected as a polypeptide of 96 kDa and
270 EMCV infection resulted in the appearance of an 80 kDa GFP-containing protein at 6 h post
271 infection and nearly complete cleavage of EGFP-G3BP1 reached near completion at 10 h
272 post infection (Fig. 3A). Because the fusion protein contains an EGFP moiety at the
273 N-terminus of G3BP, the cleavage of G3BP1 is likely to occur at the C-terminal region of
274 G3BP1. We verified the cleavage site by using an antibody detecting the C-terminal epitope

275 of G3BP1 (Fig. S1A and B). Because the mapped cleavage site was close to that by PolioV
276 and the cleavage by PolioV is prevented by amino acid substitution within G3BP1 (Q325E)
277 (15), we therefore examined this mutant for cleavage by EMCV (Fig. 3B). We found that
278 G3BP1 Q325E was resistant to cleavage by EMCV, suggesting a common cleavage
279 mechanism. To examine whether the disruption of SG by EMCV is solely due to cleavage of
280 G3BP1, we examined other SG components, PABP, TIA-1/R, HuR and PKR, which are also
281 essential for SG formation. Fig. 3C shows that the levels of SG components with the
282 exception of G3BP1 did not change upon EMCV infection and that G3BP1 cleavage
283 coincided with the detection of EMCV proteins. Expression of EMCV 3C protease but not
284 leader protein by transfection was sufficient to reproduce G3BP1 cleavage at Q325 (Fig. 3D),
285 strongly suggesting that the cleavage is mediated by 3C protease. We next examined SG
286 formation of HeLa/G-G3BPQ325E. In sharp contrast to the cells expressing wild type
287 G3BP1 (Movie S6), HeLa/G-G3BPQ325E exhibited stable formation of SGs as judged by
288 single cell imaging (Fig. 4A and B; Movie S8) and quantification (Fig. 4C). These results
289 suggest that EMCV disrupts SGs by cleavage of G3BP1 through a similar mechanism as
290 PolioV.
291
292 **G3BP1 negatively regulates EMCV replication.** To examine the impact of SG disruption
293 on EMCV replication, we infected both HeLa/G-G3BP and HeLa/G-G3BPQ325E with
294 EMCV and analyzed viral replication by RT-qPCR (Fig. 5A). EMCV RNA recovered from
295 HeLa/G-G3BP was six fold higher compared with that of HeLa/G-G3BPQ325E. Similarly, a
296 significantly lower viral yield was observed with cells expressing G3BP1 Q325E, suggesting
297 that SG formation is critical for suppressing EMCV replication. To further confirm the
298 involvement of G3BP1, we depleted endogenous G3BP1 by siRNA-mediated knockdown
299 (Fig. 5B) and examined its effect on EMCV replication. G3BP1 knockdown caused increased

300 EMCV replication as judged by the approximate 5-fold augmentation of viral RNA and viral
301 yield (Fig. 5B). These results suggest that G3BP1 is involved in the negative regulation of
302 EMCV.
303
304 **G3BP1 is critical for EMCV-induced interferon and cytokine gene activation.** Based on
305 the above findings, we next asked how G3BP1 exerts its antiviral role. The type I interferon
306 system constitutes major innate antiviral responses, therefore we examined EMCV-induced
307 IFN-β gene activation in HeLa/G-G3BP and HeLa/G-G3BPQ325E (Fig. 6). In
308 HeLa/G-G3BP cells, IFN-β mRNA accumulated at 4 h post infection, followed by a gradual
309 decrease. However, IFN-β mRNA levels persisted in HeLa/G-G3BPQ325E after 8 h post
310 infection (Fig. 6B). In agreement with these results, the amount of IFN-β protein released
311 into the culture medium at 24 h is significantly augmented by Q325E mutation (Fig. 6A).
312 Similar enhancement of cytokine mRNA was observed for CXCL10, IL-6 and RANTES (Fig.
313 6C-E). We investigated gene activation at early time points between 0 to 4 h, and observed
314 similar activation kinetics between HeLa/G-G3BP and HeLa/G-G3BPQ325E (Fig. 7),
315 suggesting that the reduced gene activation of HeLa/G-G3BP is due to G3BP1 cleavage.
316 Q325E mutation did not affect the IFN-β gene induction in the case of IAVΔNS1, which did
317 not cause G3BP1 cleavage (Fig. 6F). Next, we examined the effects of depleting endogenous
318 G3BP1 on cytokine gene activation. As expected, knockdown of endogenous G3BP1
319 attenuated IFN-β and other cytokine gene expression (Fig. 8A-D). These results strongly
320 suggest that G3BP cleavage leads to attenuation of antiviral cytokine induction.
321 It has been well documented that MDA5 senses EMCV infection (22-25), and that
322 virus- and oxidative stress-induced SGs recruit RIG-I, MDA5 and LGP2 (12). Therefore, we
323 hypothesized that EMCV-induced SG regulates IFN-β gene activation by facilitating MDA5
324 activation. We examined MDA5 localization in EMCV-infected HeLa cells by

325 immunostaining. MDA5 displayed re-localization to speckle-like granules upon EMCV
326 infection (Fig. 9A). The speckles also contain endogenous G3BP1 (Fig. 9A) and TIAR (Fig.
327 9B). Interestingly, PI, a dye that binds to dsDNA and dsRNA, stains cytoplasmic speckles
328 found only in virus-infected cells and the dsRNA speckles are co-localized with G3BP1 and
329 TIAR. These observations suggest that EMCV infection induces SGs, which recruit SG
330 markers, MDA5 and EMCV dsRNA.

331

332 **PKR is essential for SG-formation and IFN-induction in EMCV infection.** Various types
333 of viruses were shown to induce SG formation through PKR activation (26-28). We
334 therefore examined whether EMCV induces SG formation in a PKR-dependent manner.
335 Endogenous PKR expression was efficiently downregulated by siRNA (Fig. 10A). Under
336 these conditions, SG formation by EMCV was decreased significantly (Fig. 10A). We next
337 asked whether cleavage of G3BP1 results in PKR dephosphorylation. Immunoblot analyses
338 showed that PKR was autophosphorylated at 4 h post infection, however at 12 h, when
339 G3BP1 cleavage was nearly complete, PKR phosphorylation was undetectable (Fig. 10B,
340 Lane 3), suggesting that G3BP1 cleavage resulted in PKR dephosphorylation. Finally, we
341 examined whether the final outcome of the signaling, IFN-β gene expression, was dependent
342 on PKR. In PKR knockdown cells, the induction of IFN-β mRNA by EMCV was
343 significantly decreased compared to control cells (Fig. 10C). We further confirmed previous
344 reports that IFN induction by PolyI:C or IAVΔNS1 infection was PKR dependent (12). From
345 the data presented above, we concluded that loss of PKR impaired EMCV-induced SG
346 formation, leading to a reduction of IFN-β gene activation.

347

348 **DISCUSSION**

349 Viral infection causes stress in host cells, resulting in SG formation. To date, both pro- and
350 anti-viral roles have been described for virus-induced SGs (28-30) and this issue remains
351 controversial.

352 In this study, we demonstrated that SGs are potentially involved in mediating
353 virus-triggered IFN responses. It was reported that PolioV 3C protease cleaves G3BP1 at the
354 residue of Q325, resulting in the disruption of SGs (15). The observation indicates that
355 G3BP1 is not only a component of SGs but also its inactivation by cleavage causes the
356 disruption of SGs. Here, we show that EMCV shares G3BP cleavage activity with identical
357 specificity to PolioV 3C requiring intact Q325. Interestingly, Coxsackie virus also disrupts
358 SG (31) by a similar mechanism (Fung et al unpublished observation), suggesting that this
359 strategy is shared by some picornaviruses to evade immune responses. At the early phase of
360 EMCV infection, cleavage of G3BP1 was not evident. However, at 4 hpi, cleavage was
361 detectable, and at 10 h, cleavage reached completion, suggesting that the accumulation of 3C
362 is necessary for the disruption. We observed that stable expression of G3BP1 Q325E blocked
363 the disassembly of SGs as well as enhanced IFN-β production at a late phase of infection.
364 Furthermore, knockdown experiments showed that G3BP1 is necessary for efficient
365 activation of the IFN-β gene, particularly at the later stages of infection. Although it was
366 reported that PolioV 3C cleaves RIG-I and MDA5 (32), and EMCV cleaves RIG-I (33), we
367 did not observe these cleavages even under the conditions in which G3BP1 was cleaved by
368 EMCV or PolioV (Fig. 11). Taken together, we conclude that G3BP1 is a physiological
369 regulator of IFN-β gene induction through the formation of SGs, which recruits the RNA
370 sensor MDA5. In addition, the persistent activation of the IFN-β gene at late time points is
371 likely due to the increase of the local concentration of both MDA5 and its ligands within the
372 condensed granules.

373 Collectively, the data presented above strongly suggest that 3C protease of EMCV
374 acts as critical factor for evading host IFN production to ensure efficient replication. It was
375 demonstrated that PKR plays a critical role in dsRNA- or IAVΔNS1-induced SG formation
376 and subsequent IFN-β gene activation (12). Our observation that PKR is required for efficient
377 IFN gene activation by EMCV, suggests that PKR is responsible for initiating the SG
378 formation (Fig. 10).
379 Considering that the assembly of SGs is a part of antiviral response of the host, it is
380 plausible that viruses evolve strategies to block it. Indeed, IAV, SeV and TMEV do not
381 induce SG (Fig. 2) and it was reported that leader RNA, NS1 and leader protein are
382 responsible for the inhibition, respectively (8,12,34). Although TMEV belongs to
383 *Picornaviridae*, their mechanism of SG inhibition appeared to be distinct from those of
384 EMCV and PolioV. TMEV and Mengovirus inhibit SG by the action of leader protein
385 (8,31). We found that 3C but not the leader protein of EMCV inhibits SG formation (Fig. 12).
386 It is tempting to speculate that leader of TMEV and Mengovirus inhibit IFN production
387 (35,36) through the blockade of SG formation, where RLR and viral RNA efficiently interact,
388 as one of the mechanisms. Interestingly, although the leader of EMCV did not affect SGs, it
389 inhibits IFN gene activation (Fig. 12), suggesting that leaders of different cardioviruses are
390 functionally equivalent (37,38), however through distinct mode of action. Therefore, these
391 viruses encode multiple inhibitory proteins to efficiently manipulate host immune responses.
392 EMCV and SINV induced SG at early time points after infection but the SG formation was
393 disrupted later. A similar phenomenon was reported for West Nile and Dengue viruses by
394 monitoring TIA-1/R as a SG marker (29). In the case of EMCV and PolioV, G3BP1 cleavage
395 by viral 3C protease is responsible for the disassembly of the SG. Therefore, active
396 mechanisms for the disruption of SGs by SINV, West Nile and Dengue viruses have been
397 suggested, although underlying mechanisms remain to be determined. In addition to transient

398 formation of SGs, some viruses exhibited alternating formation of SGs; SGs were formed at
399 an early stage then disappeared and re-formed at a later stage. This alternating pattern is also
400 dependent on the cell lines used (unpublished observation), suggesting that the pattern of SG
401 formation is determined by a dynamic balance between host antiviral response and viral
402 inhibitory mechanism (21). Such a host mechanism could be a therapeutic target to enhance
403 host defense against viruses.

404 Here we provide evidence that EMCV-induced SGs are involved in regulating IFN-β
405 gene expression. Thus, virus-induced SGs might play dual roles: (i) suppressing viral
406 replication through an inhibition of viral protein synthesis, and (ii) serving as a platform to
407 facilitate IFN-β production.

408

409 **ACKNOWLEDGEMENTS**

410 We thank Dr. Jamal Tazi for providing pEGFP-G3BP1, Dr. A.C. Palmenberg for expression
411 vectors for EMCV leader and 3C proteins, Gabriel Fung (University of British Columbia) and
412 Dr. Peter Gee (Kyoto University) for proofreading the manuscript. This research was
413 supported by the following grants. The Ministry of Education, Culture, Sports, Science and
414 Technology (MEXT) of Japan (Innovative Areas ‘‘Infection competency’’ (No.24115004),
415 Scientific Research ‘‘A’’(23249023)), the Ministry of Health, Labor and Welfare of Japan,
416 the Uehara Memorial Foundation, the Mochida Memorial Foundation for Medical and
417 Pharmaceutical Research, the Takeda Science Foundation, the Naito Foundation, and Nippon
418 Boehringer Ingelheim. N.C.S. is a recipient of Monbukagakusho fellowship from MEXT. All
419 authors declare no conflict of interest.

420

421 **REFERENCES**

422 1. **Meylan E, Tschopp J and Karin M.** 2006. Intracellular pattern recognition receptors
423 in the host response. Nature **442**:39-44.

424 2. **Darnell Jr JE, Kerr IM and Stark GR**. 1994. Jak-STAT pathways and
425 transcriptional activation in response to IFNs and other extracellular signaling
426 proteins. Science **264**:1415-1421.

427 3. **Garcia J MA, Ventoso GI, Guerra S, Domingo E, Rivas C and Esteban M**. 2006.
428 Impact of Protein Kinase PKR in Cell Biology: from antiviral to antiproliferative
429 action. Microbiol. & Mol. Biol. Reviews **70**:1032-1060.

430 4. **Der S. and Lau AS**. 1995. Involvement of the double-stranded-RNA-dependent
431 kinase PKR in interferon expression and interferon-mediated antiviral activity. Proc.
432 Natl. Acad. Sci. USA **92**:8841-8845.

433 5. **Terenzi F, DeVeer M, Ying H, Restifo NP, Williams BR and Silverman RH**. 1999.
434 The antiviral enzymes PKR and RNase L suppress gene expression from viral and
435 non-viral based vectors. Nucleic acids Research **27**:4369-4375.

436 6. **McInerney GM, Kedersha NL, Kaufman RJ, Anderson P and Liljeström P.** 2005.
437 Importance of eIF2α phosphorylation and stress granule assembly in Alphavirus
438 Translation Regulation. Mol. Biol. Cell. **16**:3753-3763.

439 7. **White, JP and Lloyd RE.** 2012. Regulation of stress granules in virus systems.
440 Trends Microbiol. **20**:175-183.

441 8. **Borghese F. and Michiels T**. 2011. The leader protein of cardioviruses inhibits stress
442 granule assembly. J. Virol. **85**:9614-9622.

443 9. **Katoh H, Okamoto T, Fukuhara T, Kamban H, Morita E, Mori Y, Kamitani W**
444 **and Matsuura Y**. 2013. Japanese Encephalitis virus core protein inhibits stress

445 granule formation through an interaction with Caprin-1 and facilitates viral
446 propagation. J. Virol. **87**:489-502.
447 10. **Okonski KM and Samuel CE**. 2013. Stress granule formation induced by measles
448 virus is protein kinase PKR-dependent and impaired by RNA Adenosine deaminase
449 ADAR1. J. Virol. **87**:756-766.
450 11. **Dinh PX, Beura LK, Das PB, Panda D, Das A and Pattnaik AK**. 2013. Induction
451 of stress granule (SG)-like structures in vesicular stomatitis virus-infected cells. J.
452 Virol. **87**:372-383.
453 12. **Onomoto K, Jogi M, Yoo JS, Narita R, Morimoto S, Takemura A, Sambhara S,**
454 **Kawaguchi A, Osari S, Nagata K, Matsumiya T, Namiki H, Yoneyama M and**
455 **Fujita T.** 2012. Critical role of an antiviral stress granule containing RIG-I and PKR
456 in viral detection and innate immunity. PLoS One **7**:e43031.
457 13. **Tourrière H, Chebli K, Zekri L, Courselaud B, Blanchard JM, Bertrand E and**
458 **Tazi J.** 2003. The RasGAP-associated endoribonuclease G3BP assembles stress
459 granules. J. Cell Biol. **160**:823-831.
460 14. **Kedersha N, Tisdale S, Hickman T and Anderson P.** 2008. Real-Time and
461 quantitative imaging of mammalian stress granules and processing bodies. Methods in
462 Enzymology **448**:521-552.
463 15. **White JP, Cardenas AM, Marissen WE and Lloyd RE**. 2007. Inhibition of
464 cytoplasmic mRNA stress granule formation by a viral proteinase. Cell Host Microbe
465 **15**:295-305.
466 16. **Porter FW, Bochkov YA, Albee AJ, Wiese C. and Palmenberg AC**. 2006. A
467 picornavirus protein interacts with Ran-GTPase and disrupts nucleocytoplasmic
468 transport. Proc. Natl. Acad. Sci. USA **103**:12417-12422.

469 17. **Ouda R, Onomoto K, Takahasi K, Edwards MR, Kato H, Yoneyama M and**
470 **Fujita T.** 2011. Retinoic acid-inducible gene I-inducible miR-23b inhibits infections
471 by minor group rhinoviruses through down-regulation of the very low density
472 lipoprotein receptor. J. Biol. Chem. **286**:26210-26219.
473 18. **Garcia-Sastre A, Egorov A, Matassov D, Brandt S, Levy DE, Durbin JE, Palese P**
474 **and Muster T.** 1998. Influenza A virus lacking the NS1 gene replicates in
475 interferon-deficient systems. Virology **252**:324-330.
476 19. **Tisoncik JR, Billharz R, Burmakina S, Belisie SE, Proll SC, Korth MJ,**
477 **Garcia-Sastre A and Katze MG.** 2011. The NS1 protein influenza A virus suppresses
478 interferon-regulated activation of antigen-presentation and immune-proteasome
479 pathways. J. Gen. Virol. **92**:2093-2104.
480 20. **Kharraz Y, Salmand PA, Camus A, Auriol J, Gueydan C, Kruys V and Morello**
481 **D.** 2010. Impaired embryonic development in mice overexpressing the RNA-binding
482 TIAR. PLoS One **5**:e11352.
483 21. **Ruggieri A, Dazert E, Metz P, Hofmann S, Bergeest JP, Mazur J, Bankhead P,**
484 **Hiet MS, Kallis S, Alvisi G, Samuel CE, Lohmann V, Kaderali L, Rohr K, Frese**
485 **M, Stoecklin G and Bartenschlager R.** 2012. Dynamic oscillation of translation and
486 stress granule formation mark the cellular response to virus infection. Cell Host
487 Microbe **12**:71-85.
488 22. **Kato H, Sato S, Yoneyama M, Yamamoto M, Uematsu S, Matsui K, Tsujimura T,**
489 **Takeda K, Fujita T, Takeuchi O and Akira S**. 2005. Cell type-specific involvement
490 of RIG-I in antiviral response. Immunity **23**:19-28.
491 23. **Kato H, Takeuchi O, Sato S, Yoneyama M, Yamamoto M, Matsui K, Uematsu S,**
492 **Jung A, Kawai T, Ishii KJ, Yamaguchi O, Otsu K, Tsujimura T, Koh CS, Reis e**

493 **Sousa C, Matsuura Y, Fujita T and Akira S.** 2006. Differential roles of MDA5 and
494 RIG-I helicases in the recognition of RNA viruses. Nature **441:**101-105.
495 24. **Ng CS, Kato H and Fujita T**. 2012. Recognition of viruses in the cytoplasm by
496 RLRs and other helicases-how conformational changes, mitochondrial dynamics and
497 Ubiquitination control innate immune responses. Int. Immunol. **24**:739-749.
498 25. **Feng Q, Hato SV, Langereis MA, Zoll J, Virgen-Slane R, Peisley A, Hur S,**
499 **Semler BL, van Rij RP and van Kuppeveld FJ.** 2012. MDA5 detects the
500 double-stranded RNA replicative form in picornavirus-infected cells. Cell Rep
501 **2**:1187-1196.
502 26. **Lindquist ME, Mainou BA, Dermody TS and Crowe JE Jr.** 2011. Activation of
503 protein kinase R is required for induction of stress granules by respiratory syncytial
504 virus but dispensable for viral replication. Virology **413**:103-110.
505 27. **Khaperskyy DA, Hatchette TF and McCormick C.** 2012. Influenza A virus inhibits
506 cytoplasmic stress granule formation. FASEB J. **26**:1629-1639.
507 28. **Simpson-Holley M, Kedersha N, Dower K, Rubins KH, Anderson P, Hensley LE**
508 **and Connor JH.** 2011. Formation of antiviral cytoplasmic granules during
509 orthopoxvirus infection. J. Virol. **85**:1581-1593.
510 29. **Emara MM and Brinton MA.** 2007. Interaction of TIA-1/TIAR with West Nile and
511 dengue virus products in infected cells interferes with stress granule formation and
512 processing body. Proc. Natl. Acad. Sci. USA **104**:9041-9046.
513 30. **Qin Q, Hastings C and Miller CL.** 2009. Mammalian orthoreovirus particles induce
514 and are recruited into stress granules at early times postinfection. J. Virol.
515 **83**:11090-11101.

516 31. **Langereis MA, Feng Q and van Kuppeveld FJ.** 2013. MDA5 localizes to stress
517 granules but this localization is not required for the induction of type I interferon. J.
518 Virol. (doi: 10.1128/JVI.03213-12).
519 32. **Barral PM, Morrison JM, Drahos J, Gupta P, Sarker D, Fisher PB and**
520 **Racaniello VR.** 2007. MDA-5 is cleaved in Poliovirus-infected cells. J. Virol.
521 **81**:3677-3684.
522 33. **Barral PM, Sarkar D, Fisher PB and Racaniello VR.** 2009. RIG-I is cleaved
523 during picornavirus infection. Virology **391**:171-176.
524 34. **Iseni F, Garcin D, Nishio M, Kedersha N, Anderson P and Kolakofsky D.** 2002.
525 Sendai virus trailer RNA binds TIAR, a cellular protein involved in virus-induced
526 apoptosis. The EMBO J **21**:5141-5150.
527 35. **Ricour C, Delhaye S, Hato SV, Olenyik TD, Michel B, van Kuppeveld FJ, Gustin**
528 **KE and Michiels T.** 2009. Inhibition of mRNA export and dimerization of interferon
529 regulatory factor 3 by Theiler's virus leader protein. J Gen Virol. **90**:177-186.
530 36. **Delhaye S, van Pesch V and Michiels T**. 2004. The leader protein of Theiler's virus
531 interferes with nucleocytoplasmic trafficking of cellular proteins. J. Virol.
532 **78**:4357-4362.
533 37. **Paul S and Michiels T.** 2006. Cardiovirus leader proteins are functionally
534 interchangeable and have evolved to adapt to virus replication fitness. J. Gen Virol.
535 **87**:1237-1246.
536 38. **Hato SV, Ricour C, Schulte BM, Lanke KH, de Bruijni M, Zoll J, Melchers WJ,**
537 **Michiels T and van Kuppeveld FJ.** 2007. The mengovirus leader protein blocks
538 interferon-alpha/beta gene transcription and inhibits activation of interferon regulatory
539 factor 3. Cell Microbiol. **9**:2921-2930.

540

Figure Legends

FIG 1. Characterization of HeLa/G-G3BP cells. (A) HeLa/G-G3BP1 clone 12 was mock treated or stimulated as indicated. Cells were fixed and examined for GFP fluorescence. Four independent HeLa/G-G3BP cell clones were stimulated by arsenite (B) or by infection with NDV (C) and % of GFP speckle positive cells was determined. (D) Parental HeLa cells and HeLa/G-G3BP1 clones were infected with NDV for 12 h and IFN -β gene expression was determined by RT-qPCR. (Error bars, ±S.D. of duplicates, N=2).

FIG 2. Three major forms of virus-induced stress granule distribution pattern in HeLa/G-G3BP cells infected with different viruses. HeLa/G-G3BP cells were infected with (**A**) NDV, (**B**) IAV, (**C**) IAV□NS1, (**D**) EMCV, (**E**) SINV, (**F**) PolioV, (**G**) SeV, (**H**) VSV, (**I**) adenovirus 5 with E1A deletion (Adeno5□E1A), (**J**) adenovirus 5 wild type (Adeno5WT) and (**K**) TMEV for 9~12 h and SG formation was monitored and quantified as described in materials and methods. (Error bars, ±S.D. of triplicates, n=3; N.D.-not detectable). $^{**}P<0.005$, $^{*}P<0.05$. Representative cell images taken at the indicated time after infection, for stable (**L**, NDV), transient (**M**, SINV) and alternating (**N**, Adeno5□E1A) SG formation are shown. Wild type HeLa cells were mock infected or infected for 4 or 12 h and fixed to examine localization of endogenous G3BP1 by immunostaining (**O**).

FIG 3. EMCV infection results in the cleavage of G3BP1. (**A**) Immunoblotting showing the kinetics of G3BP1 cleavage in EMCV-infected HeLa/G-G3BP1 cells. (**B**) HeLa stably expressing FLAG-G3BP1Q325E was infected with EMCV and G3BP1Q325E protein level was monitored by immunoblotting. (**C**) Western blot analysis of HeLa/G-G3BP1 cells

565 infected with EMCV. Lysates were prepared at the indicated time points after infection and
566 subjected to immunoblotting by the indicated antibodies. (**D**) HeLa cells were transiently
567 transfected with empty vector or expression vector for leader or 3C and analyzed for
568 endogenous G3BP1 by Western blotting (left). HeLa/G-G3BP1 and HeLa/G-G3BP1Q325E
569 were transiently transfected with empty vector or expression vector for leader or 3C and
570 analyzed by Western blotting using anti GFP (right).

571

572 **FIG 4. HeLa/G-G3BPQ325E cells displayed stable formation of SG induced by EMCV**
573 **infection.** Both HeLa/G-G3BP1 (**A**) and HeLa/G-G3BP1Q325E (**B**) cells were infected with
574 EMCV. GFP fluorescence image of these cells at every 40 min is shown. (**C**) Quantitative
575 analysis of SG formation pattern of HeLa/G-G3BP1Q325E cells infected with EMCV. (Error
576 bars, ±S.D. of triplicates, n=3; N.D.-not detectable). $^{**}P<0.005$.

577

578 **FIG 5. Cleavage or knockdown of G3BP1 results in enhanced EMCV replication.** (**A**)
579 HeLa/G-G3BP1 and HeLa/G-G3BP1Q325E cells were infected with EMCV. Total RNA was
580 harvested at 12 h post infection and EMCV RNA was quantified by qPCR (upper). The
581 culture supernatant was subjected to plaque titration (lower). (**B**) HeLa cells were either
582 transfected with control siRNA or that targeted to G3BP1. After 48 h, G3BP1 was detected
583 by Western blotting (upper left) or by staining using anti G3BP1 antibody (upper right). To
584 investigate the effect of G3BP1 knockdown on viral replication, the cells were infected with
585 EMCV for 12 h and total RNA was extracted and EMCV RNA was quantified by qPCR
586 (bottom left). The culture supernatant was analyzed for viral titer (bottom right).

FIG 6. Inhibition of G3BP1 in EMCV-infected cells results in sustained cytokine/chemokine mRNA accumulation. HeLa/G-G3BP1 and HeLa/G-G3BP1Q325E cells were infected with EMCV. Culture supernatant was subjected to ELISA for IFN-β (A). Total RNA was harvested at the indicated time points. mRNAs for (**B**) IFN-β, (**C**) CXCL10, (**D**) IL-6 and (**E**) RANTES were determined by RT-qPCR. (**F**) Both HeLa/G-G3BP and HeLa/G-G3BPQ325E cells were infected with IAV□NS1 and IFN-β mRNA was quantified as above (left). The lysate of IAV□NS1-infected HeLa/G-G3BP1 cells were examined for cleavage of G3BP1 by Western blotting (right). Data depicted are the representative of two independent experiments (Error bars, ±S.D. of duplicates). $^{**}P<0.005$, $^{*}P<0.05$.

FIG 7. IFN production and cytokine gene activation in HeLa/G-G3BP and HeLa/G-G3BPQ325E cells at early phase. HeLa/G-G3BP1 and HeLa/G-G3BP1Q325E cells were mock-treated or infected with EMCV for indicated time. Total RNA was extracted and mRNA was quantified for IFN-b (A), CXCL10 (B), IL-6 (C) and RANTES (D) by RT-qPCR.

FIG 8. Knockdown of G3BP1 attenuates EMCV-induced cytokine/chemokine gene activation. HeLa cells were either transfected with control siRNA or that targeted to G3BP1. After 48 h of incubation, cells were infected with EMCV for 12 h and total RNA was collected as indicated. mRNAs for (**A**) IFN-β, (**B**) RANTES, (**C**) CXCL10 and (**D**) IL-6 were determined by RT-qPCR. Data are representative of two independent experiments. (Error bar, ±S.D. of duplicates, N=2). $^{*}P<0.05$.

610 **FIG 9. EMCV infection recruits MDA5 into SGs.** HeLa cells were mock-treated or
611 infected with EMCV (MOI: 10) and fixed. The cells were stained for MDA5, G3BP1 and PI
612 (A) or MDA5, TIAR and PI (B).

613

614 **FIG 10. Involvement of PKR in EMCV-induced SG and IFN-β gene activation.** (A)
615 Knockdown of PKR expression results in reduced SGs. HeLa cells transfected with siRNA
616 targeting PKR for 48 h was examined for PKR expression by Western blotting (left). The
617 cells were infected with EMCV for 6 h and stained for endogenous G3BP1 (middle).
618 SG-containing cells were quantified (right). (B) HeLa cells infected with EMCV for 0, 4 and
619 12 h were analyzed for G3BP1, phospho-PKR, EMCV proteins and actin by immunoblotting.
620 (**C**) HeLa cells transfected with siRNA targeting PKR for 48 h was mock treated or
621 transfected with poly I:C or infected with IAVΔNS1 or with EMCV. After 12 h, IFN mRNA
622 was quantified by RT-qPCR $^{**}P<0.005$, $^{*}P<0.05$.

623

624 **FIG 11. RIG-I was not cleaved after EMCV or PolioV infection.** (A) HeLa cells were
625 either mock treated or infected with EMCV for indicated time. RIG-I was detected by
626 Western blotting. (B) HeLa cells were mock treated or infected with Polio V for 9 h.
627 G3BP1 (left) and RIG-I (right) were examined by Western blotting.

628

629 **FIG 12. EMCV 3C, but not leader inhibits SG.** (A) HeLa/G-G3BP1 and
630 HeLa/G-G3BP1Q325E were transiently transfected with empty vector or expression vector
631 for leader or 3C for 48 h. Cells were treated with 0.5 mM Sodium arsenite for 30min, fixed
632 and stained for TIAR, a SG marker. (B) HeLa cells were transiently transfected with empty

633 vector or expression vector for leader or 3C (0μg, 2μg and 4μg) for 48 h. Cells were mock

634 treated or transfected with long polyI:C (2μg/μL) for 12 h. Total RNA was collected and

635 mRNA for IFN-β was determined using RT-qPCR. Data are representative of three

636 independent experiments. (Error bar, ±S.D. of duplicates, N=3).

637

638

Supplemental FIG S1.

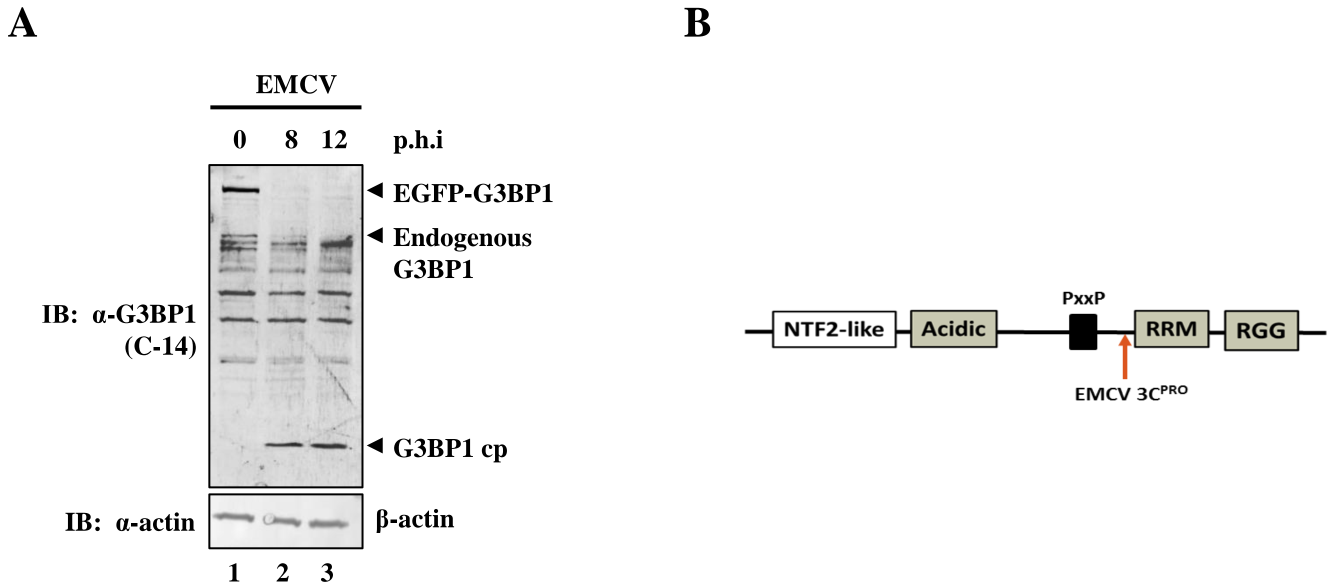

FIG S1. Detection of C-terminal cleavage product of G3BP. HeLa/G-G3BP1 cells were either mock treated or infected with EMCV. (**A**) Cell lysate was prepared at 0, 8, 12 h post infection and analyzed by Western blotting using antibodies against C-terminal region of G3BP1 or b-actin. (**B**) Cleavage site within the domain structures of G3BP1.

Supplemental Movie Legends

Movie S1. Real-time imaging of stress-granule marker, G3BP1 after NDV infection. HeLa/G-G3BP cells were either mock-treated or infected with NDV. Live-cell imaging was initiated after 1 h post-infection with images captured every 10 min. Fluorescence images at indicated time after infection are shown.

Movie S2. Real-time imaging of stress-granule marker, G3BP1 after IAVΔNS1 infection. HeLa/G-G3BP cells were either mock-treated or infected with IAVΔNS1. Live-cell imaging was initiated after 1 h post-infection with images captured every 10 min. Fluorescence images at indicated time after infection are shown.

Movie S3. Real-time imaging of stress-granule marker, G3BP1 after Adeno5WT infection. HeLa/G-G3BP cells were either mock-treated or infected with Adeno5WT. Live-cell imaging was initiated after 1 h post-infection with images captured every 10 min. Fluorescence images at indicated time after infection are shown.

Movie S4. Real-time imaging of stress-granule marker, G3BP1 after SINV infection. HeLa/G-G3BP cells were either mock-treated or infected with SINV. Live-cell imaging was initiated after 1 h post-infection with images captured every 10 min. Fluorescence images at indicated time after infection are shown.

Movie S5. Real-time imaging of stress-granule marker, G3BP1 after PolioV infection. HeLa/G-G3BP cells were either mock-treated or infected with PolioV (MOI=1). Live-cell imaging was initiated after 1 h post-infection with images captured every 10 min. Fluorescence images at indicated time after infection are shown.

Movie S6. Real-time imaging of stress-granule marker, G3BP1 after EMCV infection. HeLa/G-G3BP cells were either mock-treated or infected with EMCV (MOI=10). Live-cell imaging was initiated after 1 h post-infection with images captured every 10 min. Fluorescence images at indicated time after infection are shown.

Supplemental Movie Legends

Movie S7. Real-time imaging of stress-granule marker, G3BP1 after Adeno5ΔE1A infection. HeLa/G-G3BP cells were either mock-treated or infected with Adeno5ΔE1A. Live-cell imaging was initiated after 1 h post-infection with images captured every 10 min. Fluorescence images at indicated time after infection are shown.

Movie S8. Real-time imaging of stress-granule marker, G3BPQ325E mutant stable cells after EMCV infection. HeLa/G-G3BPQ325E cells were either mock-treated or infected with EMCV (MOI=10). Live-cell imaging was initiated after 1 h post-infection with images captured every 10 min. Fluorescence images at indicated time after infection are shown.

Movie S9. Real-time imaging of stress-granule marker, G3BP1 after TMEV infection. HeLa/G-G3BP cells were either mock-treated or infected with TMEV (MOI=10). Live-cell imaging was initiated after 1 h post-infection with images captured every 10 min. Fluorescence images at indicated time after infection are shown.

FIG S1. Detection of C-terminal cleavage product of G3BP. HeLa/G-G3BP1 cells were either mock treated or infected with EMCV. (**A**) Cell lysate was prepared at 0, 8, 12 h post infection and analyzed by Western blotting using antibodies against C-terminal region of G3BP1 or b-actin. (**B**) Cleavage site within the domain structures of G3BP1.

FIG. 1

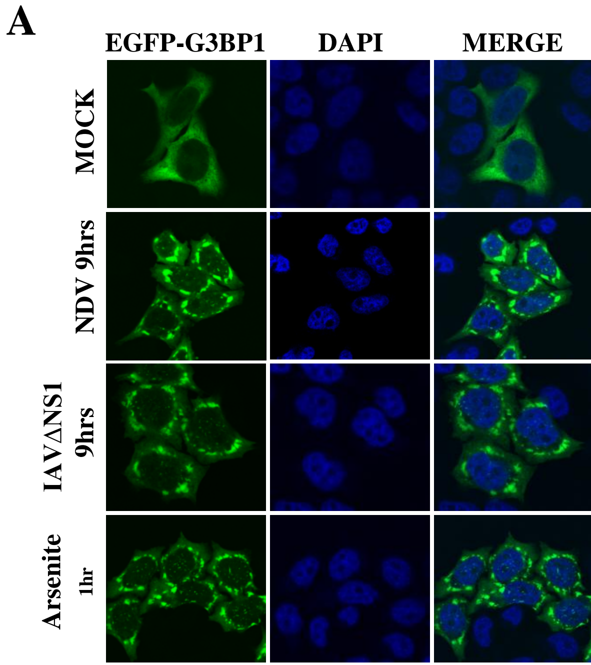

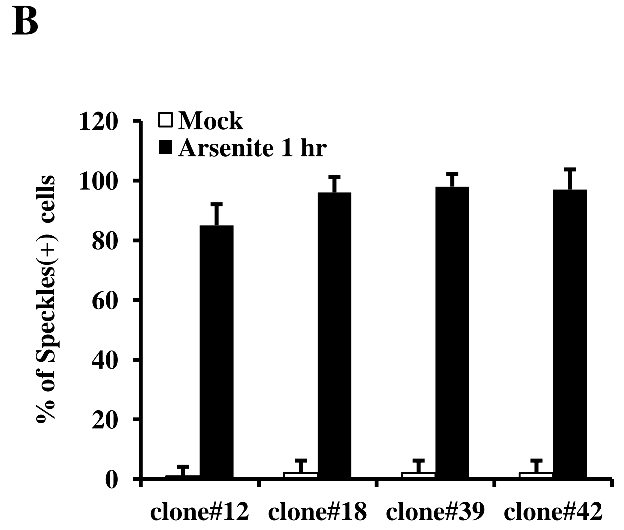

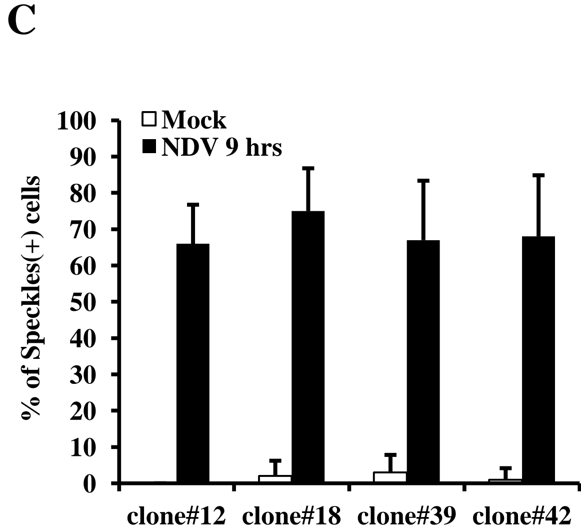

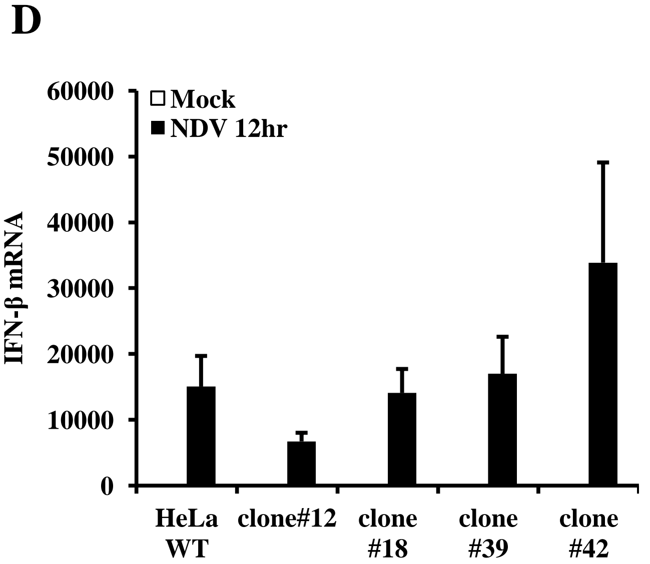

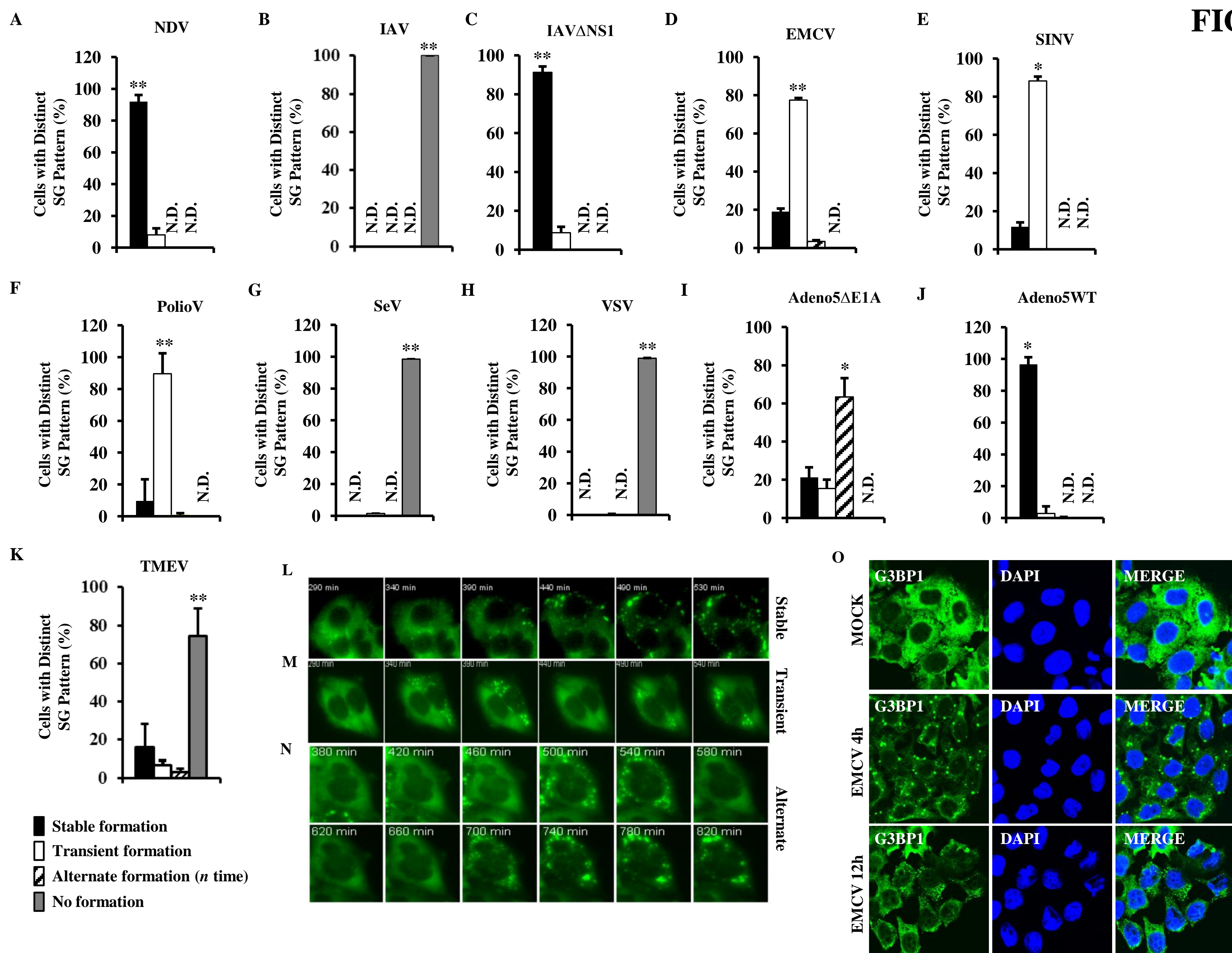
FIG. 2
A
NDV
B
IAV
C
IAVΔNS1
D
EMCV
E
SINV
F
PolioV
G
SeV
H
VSV
I
Adeno5ΔE1A
J
Adeno5WT
K
TMEV
Cells with Distinct SG Pattern (%)
N.D.
**
*
L
M
N
O
Stable
Transient
Alternate
290 min
340 min
390 min
440 min
490 min
530 min
540 min
380 min
420 min
460 min
500 min
540 min
580 min
620 min
660 min
700 min
740 min
780 min
820 min
G3BP1
DAPI
MERGE
MOCK
EMCV 4h
EMCV 12h
Stable formation
Transient formation
Alternate formation (n time)
No formation

FIG. 3

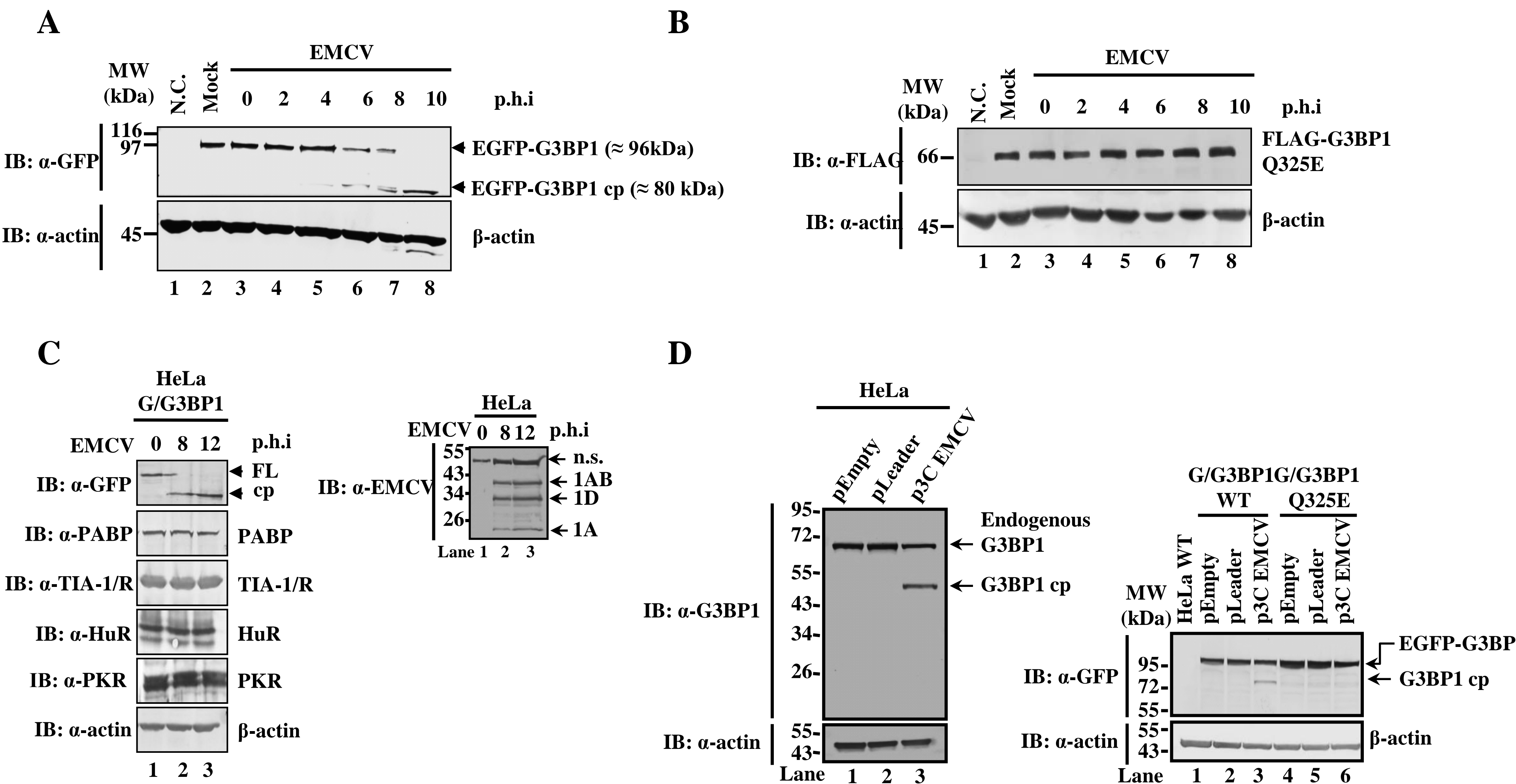

FIG. 4

A

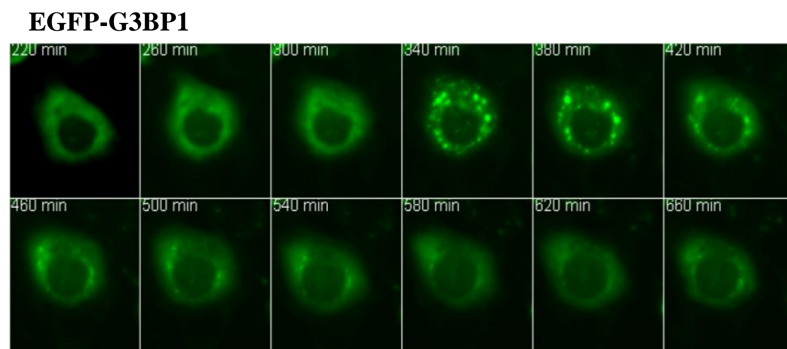

B

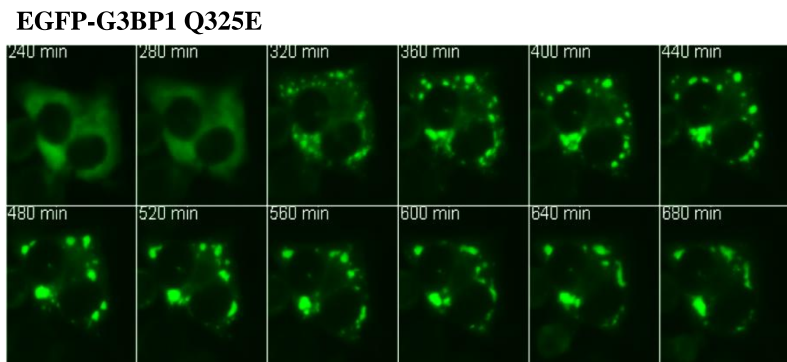

C

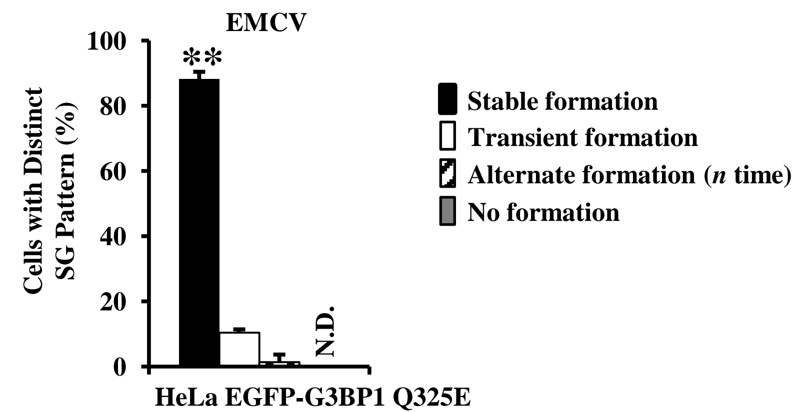

FIG. 5

A

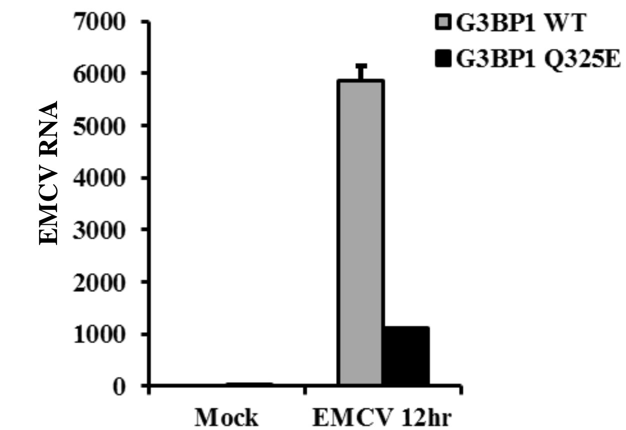

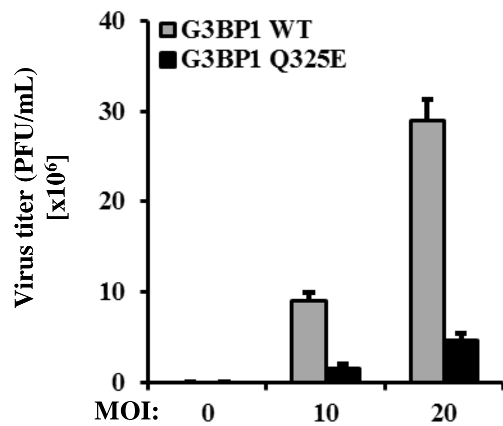

B

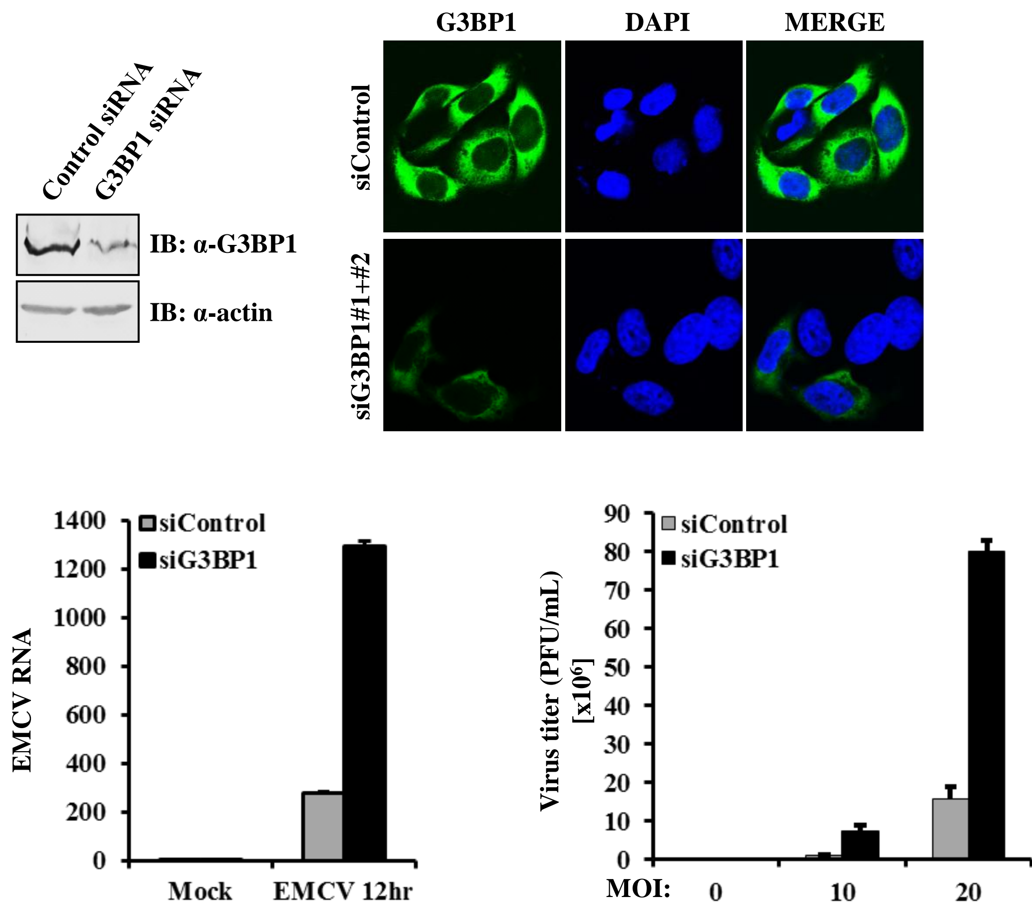

FIG. 6

A

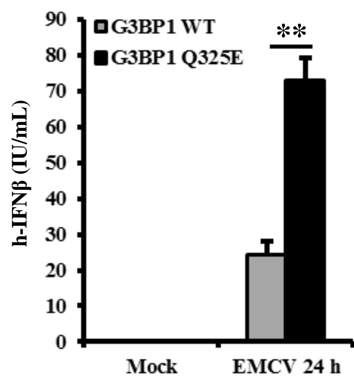

B

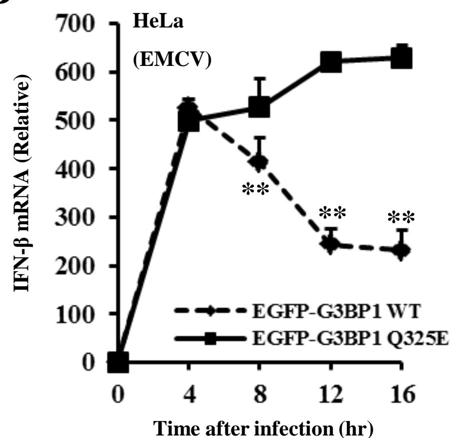

C

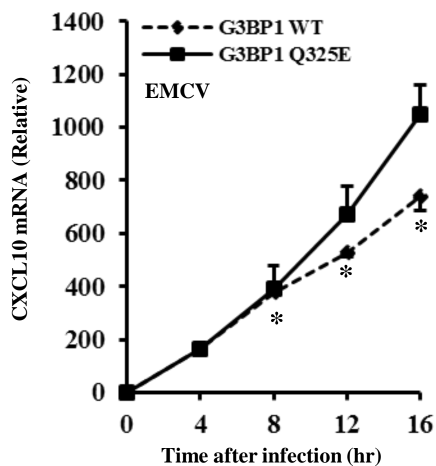

D

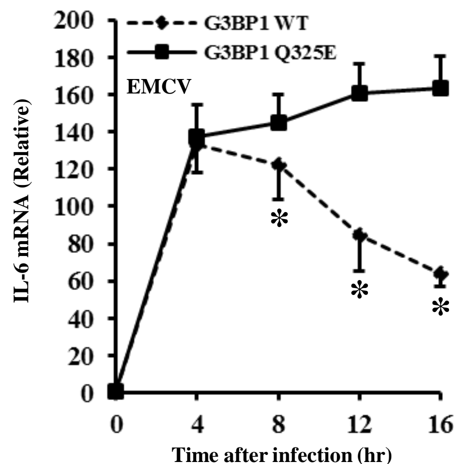

E

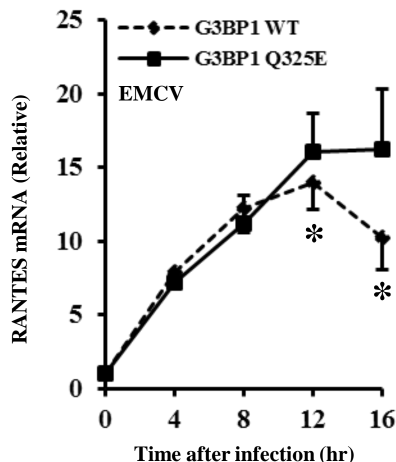

F

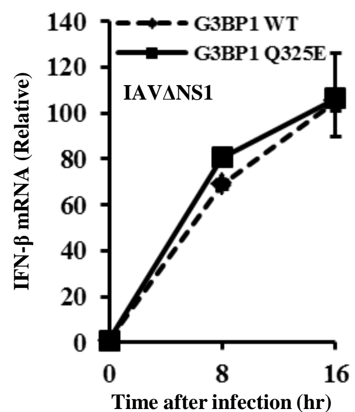

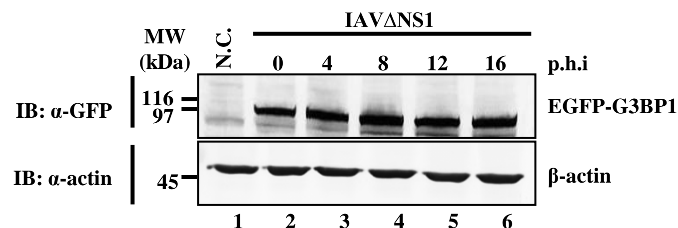

FIG. 7

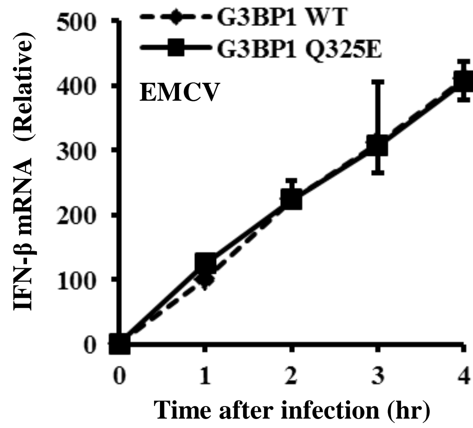

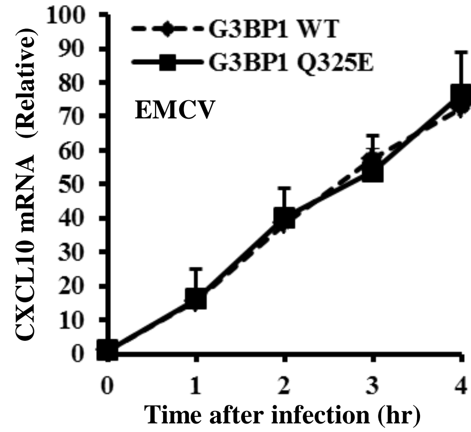

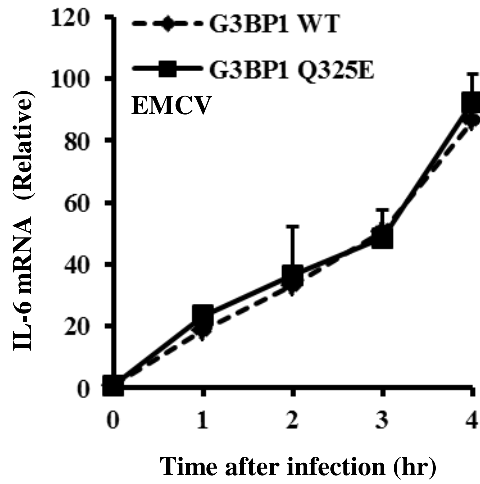

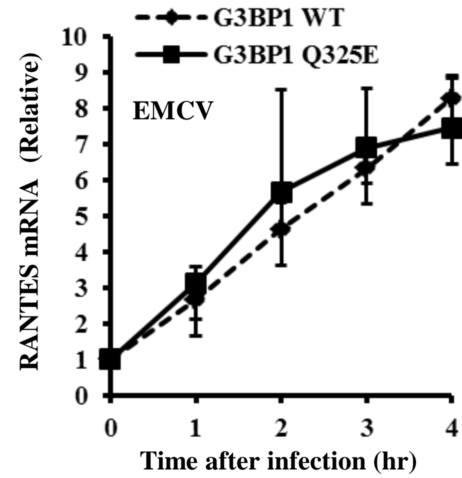

FIG. 8

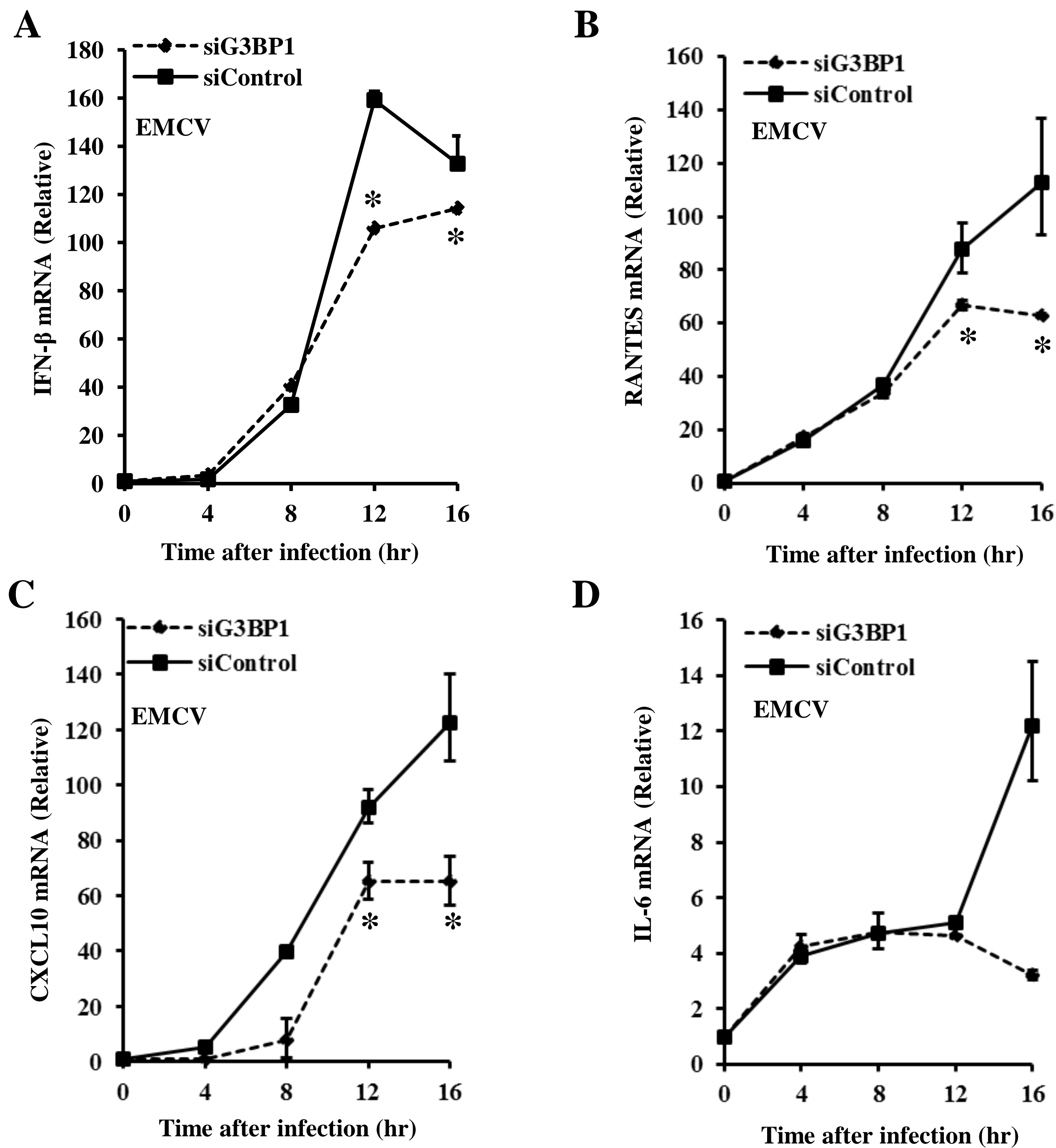

FIG. 9

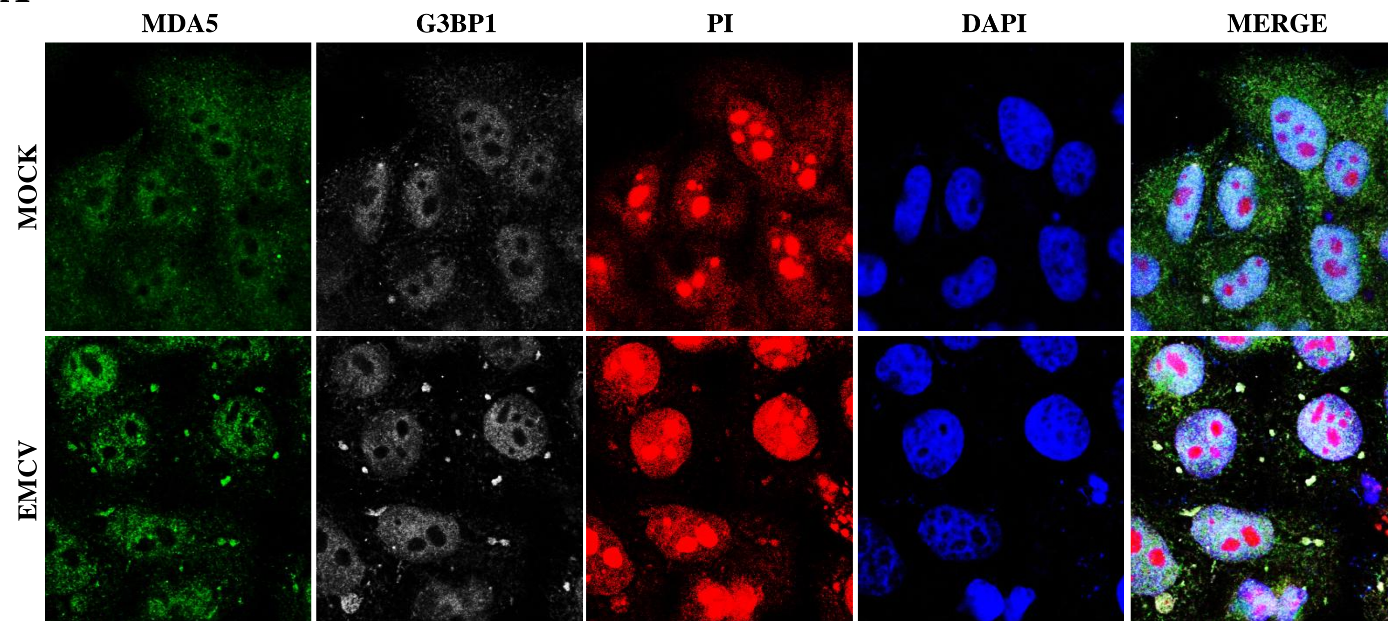

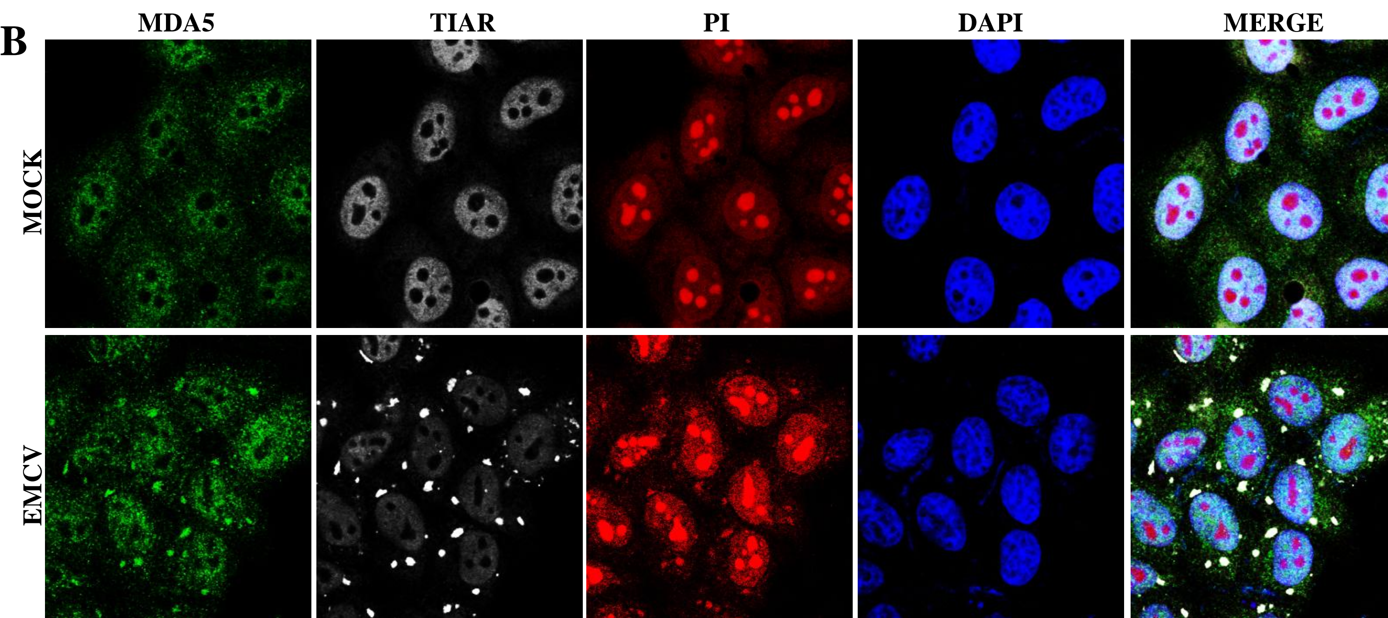

FIG. 10

A

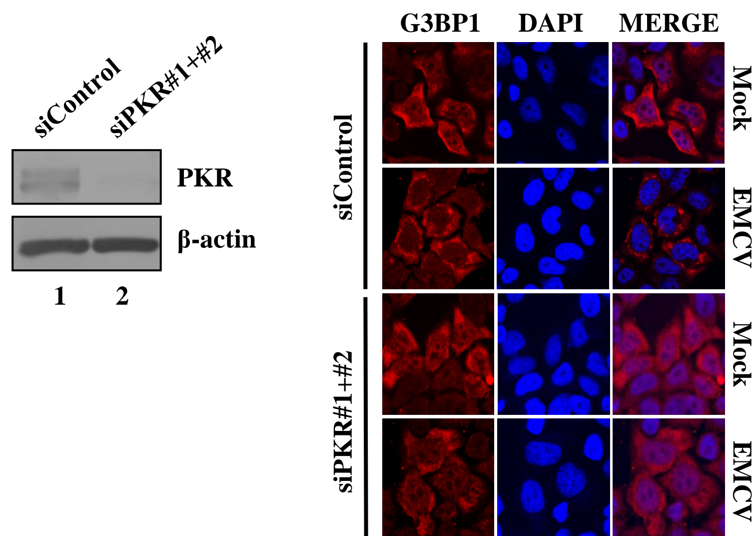

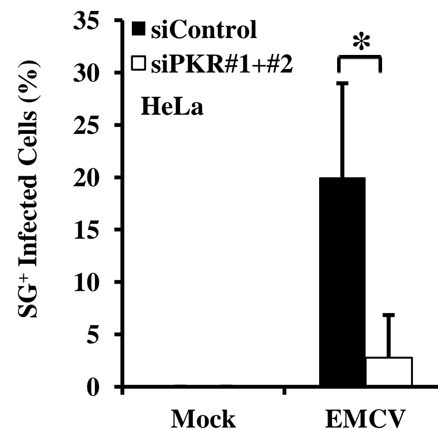

B

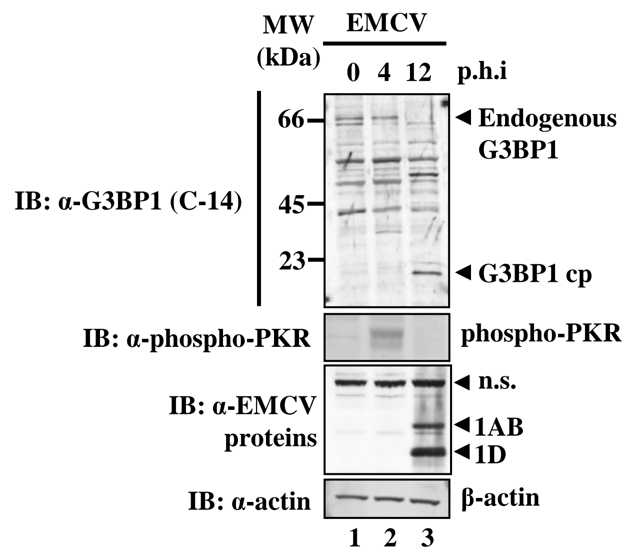

C

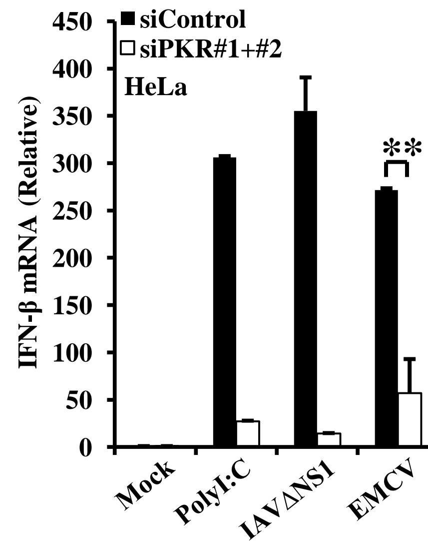

FIG. 11

A

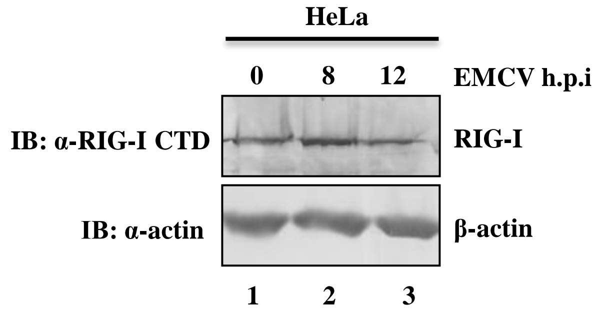

B

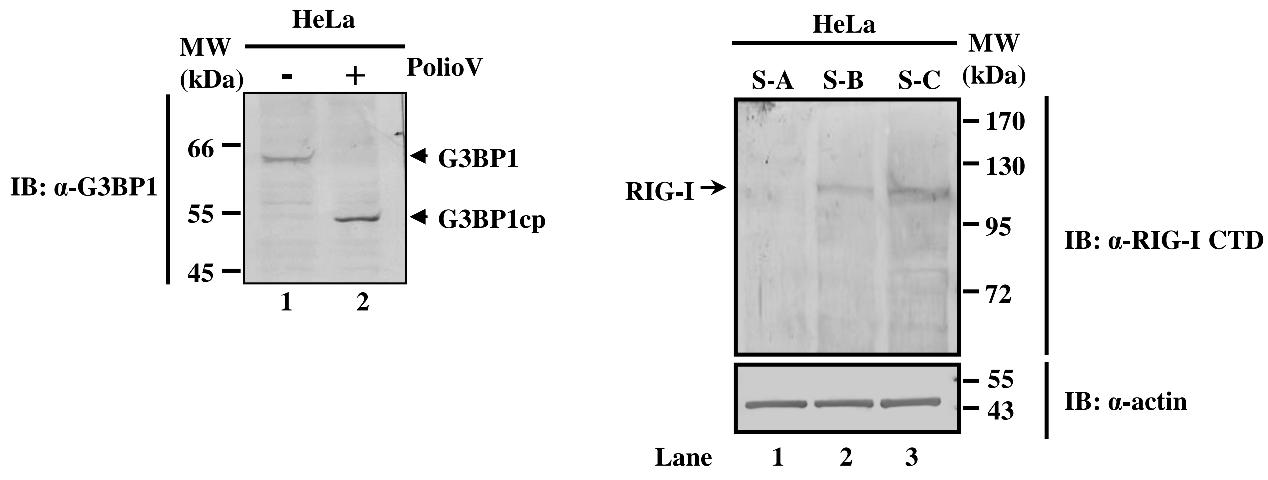

Note:
S-A: Mock with shRIG-I
S-B: Mock infection
S-C: PolioV 9 h

FIG. 12

A

G/G3BP1 WT | TIAR | DAPI | MERGE

pEmpty: MOCK; ARSENITE 30min

pLeader: MOCK; ARSENITE 30min

p3C EMCV: MOCK; ARSENITE 30min